Materials Advances

Accepted Manuscript

This article can be cited before page numbers have been issued, to do this please use: A. Kumar Samuel, Z. Ertekin, F. Walton, W. Li, F. Tierney, I. Maini, C. Kelly, S. Watson, D. A. J. Moran, I. Zeimpekis, M. D. Symes and A. Y. Ganin, *Mater. Adv.*, 2026, DOI: 10.1039/D6MA00277C.

ROYAL SOCIETY OF CHEMISTRY

rsc.li/materials-advances

View Article Online
DOI: 10.1039/D6MA00277C

Ultra-Thin Ru-Sputtered on Ti-Felt Gas Diffusion Layer as Anode for Proton Exchange Membrane Electrolyzer

Arun Kumar Samuel[a], Zeliha Ertekin[a], Finlay Walton[b], Weihao Li[a], Finn Tierney[a], Isha Maini[b], Christopher Kelly[a], Scott Watson[b], David Moran[b], Ioannis Zeimpekis[c,d], Mark D. Symes[a], Alexey Y. Ganin[a]*

[a] *WestCHEM, School of Chemistry, University of Glasgow, University Avenue, Glasgow G12 8QQ, United Kingdom*

[b] *James Watt School of Engineering, University of Glasgow, University Avenue, Glasgow G12 8QQ, United Kingdom*

[c] *School of Electronics and Computer Science, University of Southampton, Southampton, United Kingdom*

[d] *Optoelectronics Research Centre, University of Southampton, Southampton, United Kingdom*

**Corresponding Author: alexey.ganina@glasgow.ac.uk*

Abstract

Catalyst-coated (CC) gas-diffusion layers (GDLs) are emerging as a promising way to exert more direct control over catalyst loading in proton exchange membrane water electrolysis (PEMWE). While Ru-based catalysts are recognized for their strong oxygen evolution reaction (OER) activity, their behaviour at low loadings in operational PEM electrolyzers remains scarcely explored. A GDL supported approach permits Ru to be used as a thin and precisely defined layer, but little is known about how such coatings evolve beyond the as-sputtered state, including the influence of annealing in different atmospheres. In this work, ultrathin CC GDLs were obtained by directly sputtering metallic Ru onto Ti felt, yielding well-defined 130 nm layers with a Ru loading of only 0.162 mg cm^{-2}. The effects of annealing temperature and atmosphere (Ar or Air) were investigated to determine the highest crack-free temperature achievable for the sputtered Ru coatings. Both the as prepared and annealed Ru thin films were then evaluated first in a three-electrode half-cell to assess how thermal treatment influences electrochemical performance. Among all coatings, the one annealed in air at 400 ^{o}C showed the best performance. This sample was therefore selected for full-cell PEM electrolyzer evaluation and was compared with RuO_2 sprayed onto the same Ti GDL at a much higher Ru loading of 1.8 mg cm^{-2}. The ultrathin sputtered coating (0.162 mg Ru cm^{-2}) delivered a reasonable overall performance reaching current density of 300 mA cm^{-2} versus 400 mA cm^{-2} for RuO_2 coating. Although stability constraints remain, this work shows that ultrathin sputtered Ru layers, even at extremely low loadings, hold significant promise for the development of next-generation electrolyzer catalysts.

View Article Online
DOI: 10.1039/D6MA00277C

1. Introduction

Enhancing proton exchange membrane water electrolysis (PEMWE) performance during dynamic operation is increasingly important because electricity use is the main driver of hydrogen cost, and effective catalyst utilisation is crucial for sustaining high efficiency. [1] The design of electrodes, which includes oxygen evolution catalyst distribution on the perfluorosulfonic acid (PFSA) ionomers, governs PEM electrolyzer performance by controlling proton transport, interfacial kinetics, and mass transfer. [1, 2] However, the efficiency of PEM electrolyzer is governed by the high potentials required for the oxygen evolution reaction (OER) at the anode, causing the reliance on scarce noble metals for catalyst layers.[3, 4] Ru-based metal composite catalysts [5] have been widely explored as an alternative to low-Ir-systems [6] [4], and various engineering strategies[7] were developed to confine Ru to the electrochemically active interface in acidic conditions. Despite these developments, understanding of the electrochemical behaviour of pure Ru in both half-cell and full PEM electrolyzer remains limited. For example, it can be integrated within stable and conductive oxide supports. Thin or graded catalyst layers can maximize Ru utilization while limiting exposure to unstable high-potential regions has been reported as well. Previous reports utilize carbon felt as a catalyst-coated substrate for depositing noble metals[8, 9]. However, carbon felt-based substrates can be susceptible to oxidation and corrosion under the highly anodic potentials encountered during the OER, which may limit their direct applicability to PEM water electrolyzer anodes. Thus, electrode architecture and catalyst integration play a decisive role in achieving both high performance and long-term stability in Ru-based OER electrodes. [10-12]

Conventionally, PEM electrolyzers employ catalyst-coated membranes (CCMs), where the catalyst layer is directly integrated with the Nafion membrane to ensure efficient proton transport and low interfacial resistance through intimate catalyst–ionomer–membrane contact.[2, 13] Although CCMs typically deliver superior electrochemical performance, they are also prone to degradation under harsh operating conditions and present challenges related to fabrication sensitivity, mechanical stability, and recyclability.[14] As an alternative, catalyst-coated substrates (CCS) architectures deposit the catalyst directly onto a porous conductive support (e.g., titanium felt or carbon cloth), which is then assembled with an uncoated membrane.[13] This approach can reduce or eliminate ionomer use and simplifying manufacturing compared to CCM-based configurations.[15, 16]

Several studies have explored CCS architectures using Ir and Ru electrocatalysts. Lee et al., [17] provide an overview of CCS fabrication, including spray coating of catalysts and ionomer optimization on gas diffusion substrates. Substrate-driven studies, such as Cho et al., show that direct deposition of IrO_x on Ti substrates significantly influences OER activity and stability, emphasizing the importance of catalyst–substrate interactions.[18] Despite these advances, achieving consistent performance and durability under practical operating conditions remains challenging.[2] A recent comparative report showed that neither CCM nor CCS configurations are universally superior. Instead, their performance

View Article Online
DOI: 10.1039/D6MA00277C

depends strongly on electrode architecture, catalyst type, and operating conditions, with a trade-off between high performance (CCM) and structural flexibility/diagnostic accessibility (CCS).[19]

Magnetron sputtering has emerged as a versatile method for fabricating thin film, binder-free OER catalysts with precise composition control. Such control is particularly attractive for reducing noble metal usage in proton exchange membrane water electrolysis. Early work demonstrated that sputtered IrO_2 films exhibit significant OER activity, achieving current densities of ~ 0.3 A cm^{-2} at ~ 1.55 V in PEM electrolysis cells.[20, 21] More recently, magnetron-sputtered Ir-Ru thin-film catalysts have been directly integrated into PEM water electrolyzers, with co-sputtered low-Ir/Ru layers showing substantial activity and long-term performance in single-cell tests at practical current densities. [22, 23] Performance metrics obtained from half-cell evaluations do not always translate directly to practical electrolyzer operation. Therefore, testing in device configurations under operational conditions remains essential to assess catalyst performance in acidic environments. [24]

In this study, we investigate direct sputtering of Ru onto porous Ti-felt as CCS electrodes, focusing on the effect of post-deposition annealing in air and argon. Porous Ti-felt provides a conductive and corrosion-resistant substrate suitable for binder-free catalyst layers. The combination of sputtering and controlled annealing enables tuning of the Ru oxidation state, microstructure, and adhesion, which in turn influences OER activity, interfacial resistance, and full-cell performance. The novelty of this work lies in the systematic evaluation of pure sputtered Ru thin films in a CCS configuration under both three-electrode and single-cell PEM electrolyzer conditions, an area that has received limited attention compared with low-Ir or Ru–Ir composite systems.[4] Therefore, this work investigates pure sputtered Ru thin films on platinized Ti-felt and examines the effect of annealing atmosphere on their structure, electrochemical behaviour, and PEM water electrolysis performance. This enables a direct correlation between intrinsic electrochemical behaviour and device-level performance, providing insight into the applicability and limitations of sputtered pure Ru thin films for PEM water electrolysis.

2. Experimental details

Materials and Methods

Magnetron Sputtering of Ruthenium (Ru) on Platinized Ti-fiber Felt Substrate

Ruthenium was sputtered on one side of the platinized Ti-fiber felt substrates with a geometric area of 2.3 × 2.3 cm^2 (53-56% porosity, thickness ~ 0.25 ± 0.003 mm, Fuel Cell Store) using a magnetron sputtering system (Moorfield Nanotechnology Minilab 125) at an output power of 150 W under argon atmosphere over a duration of 30 minutes. The sputtering power was selected based on prior laboratory optimization to ensure stable plasma operation and reproducible deposition of uniform Ru thin films on porous Ti-felt substrates. This setting provides a balanced deposition rate while avoiding non-uniform coating at lower powers and excessive target heating or surface roughening at higher powers. The power was kept constant for all samples to ensure experimental comparability. The chamber was evacuated to

View Article Online
DOI: 10.1039/D6MA00277C

a base pressure of approximately ~ 5×10^{-7} mbar, followed by the introduction of argon gas. The argon flow was set to 20 sccm, resulting in a working pressure of approximately ~ 3×10^{-3} mbar during deposition. The target-to-substrate distance was approximately 8 cm, and all depositions were carried out at room temperature without intentional substrate heating. Substrate rotation was used throughout deposition to enhance film uniformity across the porous Ti-felt substrates. Prior to deposition, the platinized Ti-felt substrates were ultrasonically cleaned in acetone (ACS reagent, ≥ 99.5%, Merck) for 15 min followed by deionized water for 5 min. After cleaning, the samples were dried under a nitrogen stream at room temperature and promptly transferred to the sputtering chamber to minimize exposure to ambient conditions prior to deposition. No additional surface treatment or reduction step was performed before sputtering. The Ru-target was custom designed and supplied by Moorfield Nanotechnology (99.95 % purity, 3-inch diameter, 1 mm thickness). The thickness of the sputtered Ru films was determined by atomic force microscopy (AFM, Bruker Dimension Icon). Due to the high porosity and surface roughness of the Pt/Ti-felt substrate, direct thickness measurements on Ti-felt are not reliable. Therefore, a 1×1 cm^2 SiO_2/Si reference substrate (300 nm thermal oxide) was co-deposited alongside the Pt/Ti-felt during sputtering. The Ru film thickness was then measured on this reference substrate, yielding a uniform thickness of approximately 130 ± 10 nm, allowing estimation of the Ru catalyst loading at 0.162 mg cm^{-2} (based on this thickness). This Ru-sputtered, platinized titanium felt, annealed in air and argon gas environments, was utilized as catalyst and anode gas diffusion layer in PEM water electrolyser.

Annealing of Ru sputtered Ti-Felt electrode in air and Ar-gas environment

After deposition, the larger Ru sputtered Pt/Ti-felt substrates (~ 2.3×2.3 cm^2) were cut into smaller area of ~ 0.5×0.5 cm^2. The pristine sputtered Ru thin film without any post-treatment is referred to as "as prepared". The thin-film samples (~ 0.5×0.5 cm^2) annealed at 400 °C for 3 h in air are referred to as "400 °C-Air", while those annealed at 400 °C for 3 h under argon are referred to as "400 °C-Argon". Annealing in air was carried out in a box furnace (Carbolite, ELF 1100), providing an oxidizing atmosphere, whereas annealing under argon was performed in a tubular furnace (Carbolite TZF 12/65/550) under continuous Ar flow, providing a non-oxidizing (inert) environment. In both cases, heating rates of 1 °C min^{-1} were used. After annealing, each individual Ru thin film samples were independently characterized by X-ray diffraction (XRD), scanning electron microscopy (SEM), energy-dispersive X-ray spectroscopy (EDS), X-ray photoelectron spectroscopy (XPS), and electrochemical measurements, as described in detail below.

View Article Online
DOI: 10.1039/D6MA00277C

Material Characterizations

X-ray diffraction (XRD)

XRD analyses were performed on the sputtered Ru thin film (~ 0.5 × 0.5 cm^2) samples, including as prepared films and samples annealed at 400 °C under air and argon atmospheres. Measurements were carried out using a Rigaku MiniFlex 6G diffractometer with Cu-Kα_1 and Cu-Kα_2 radiation and a D/teX Ultra detector, operated in Bragg-Brentano geometry. All the samples were affixed to a silicon zero-background holder using double-sided adhesive tape. During measurements, the samples were continuously spun at 10 rpm to improve signal uniformity. Data collection and processing were performed using Rigaku SmartLab Studio-II software (Rigaku Corporation, 2014).

X-ray photoelectron spectroscopy (XPS)

XPS measurements were conducted on the sputtered Ru thin film (~ 0.5 × 0.5 cm^2) samples. All the samples (as prepared, 400 °C Air and 400 °C Argon) were carefully placed onto an adhesive carbon tab (Agar Scientific) and mounted on the XPS sample holder. Analyses were performed using a Kratos AXIS Supra+ spectrometer with a monochromatic Al Kα X-ray source (1486.6 eV). High-resolution spectra were collected at a pass energy of 500 – 450 eV with an energy step of ~ 0.1 eV over an analyzed area of 0.66 mm^2. The C 1s peak was referenced to 284.8 eV. Data analysis was carried out using ESCApe software with Gaussian-Lorentzian fitting for the component peaks, including C 1s and Ru 3p.

Scanning electron microscopy (SEM) and energy-dispersive X-ray spectroscopy (EDS)

SEM imaging and EDS analyses were performed on the Ru thin film samples using a TESCAN CLARA microscope coupled with an Oxford Instruments UltimMax 65 detector and Aztec Live software. The as prepared, 400 °C Air and 400 °C Argon (~ 0.5 × 0.5 cm^2) samples were mounted on a carbon-adhesive disc (Agar Scientific) for imaging. The EDS data processing was carried out using Aztec software (Oxford Instruments).

Electrochemical measurements in a three-electrode configuration

Three-electrode electrochemical measurements were performed as follows. A small area (0.5 × 0.5 cm^2) of Ru sputtered Pt/Ti-felt samples (as prepared, 400 °C Air, and 400 °C Ar) were used individually as working electrodes and mounted on a clamp electrode. An Ag/AgCl electrode (saturated 3 M NaCl, CH Instruments, USA) served as the reference electrode, and carbon felt (3.18 mm thick, 99.0%, Thermo Scientific Chemicals) was used as the counter electrode. All measurements were carried out using a BioLogic SP-150 potentiostat with EC-Lab software in aqueous 0.1 M $HClO_4$ (99.99%, Thermo Scientific Chemicals). 0.1 M $HClO_4$ was selected as the electrolyte as it is a standard acidic medium for evaluating OER activity under well-defined and non-complex conditions, allowing reliable comparison of intrinsic catalyst performance.

View Article Online
DOI: 10.1039/D6MA00277C

Linear Sweep Voltammetry (LSV)

LSV polarization curves were recorded with iR compensation over the potential range of 1.0–1.65 V vs RHE at a scan rate of 5 mV s^{-1}. The electrolyte volume of 75 mL was used to ensure sufficient electrolyte depth to minimize concentration changes during measurements and to maintain stable electrochemical conditions throughout the experiment. The electrolyte was continuously stirred at 250 rpm to reduce concentration gradients near the electrode surface and to improve mass transport consistency. Nitrogen gas (99.9%, BOC) was bubbled through the electrolyte to maintain an inert atmosphere during measurements.

Cyclic Voltammetry (CV)

CV was used to evaluate the electrochemical stability and durability of the Ru thin-film samples. The measurements were conducted by cycling the potential between 1.0 and 1.65 V vs RHE for 25 cycles at a scan rate of 5 mV s^{-1} in 0.1 M $HClO_4$. The number of cycles was chosen to probe early-stage electrochemical response under repeated anodic polarization to promote electrochemical activation processes which are typically observed for Ru-based catalysts. For each cycle, the current response was recorded, and mass activity was calculated using the initial Ru loading. Comparing the mass activity across multiple cycles provides insight into the retention of catalytic performance and the structural stability of the Ru thin films under repeated potential cycling.

Chronoamperometry (CA)

CA measurements were performed at an applied potential of 3000 secs in 0.1 M $HClO_4$ under continuous stirring (250 rpm) and N_2 atmosphere at ambient temperature. The applied potential was selected based on the corresponding LSV curves, specifically at the potential where a current density of approximately 100 mA cm^{-2} was reached for the respective samples. This ensures that CA measurements are performed under a representative operating condition derived from the electrochemical response of each electrode. The current response was recorded as a function of time, and mass activity was calculated using the same approach as in the LSV measurements, normalized to the initial Ru loading. This protocol allows evaluation of the sustained catalytic activity under continuous operation and enables comparison of stability between different annealing conditions.

Inductively Coupled Plasma (ICP) Analysis

ICP analysis was conducted using an IntelliQuant screening mode, which is a rapid, semi-quantitative method based on internal calibration models within the instrument. The measurements were performed to quantify the Ru content of the sputtered Ru thin film samples (as prepared, 400 °C-Air, and 400 °C-Argon) following the CA analysis in a 3-electrode system to evaluate mass activity. For each sample, a known volume of electrolyte (15 mL aliquot) was analyzed, and the Ru concentration was determined in parts per million (ppm). The measured values were then converted to the total Ru mass in the

View Article Online
DOI: 10.1039/D6MA00277C

electrolyte and normalized to the geometric area of the film, yielding mg of Ru per cm^2 (mg_{Ru} cm^{-2}). ICP results are interpreted qualitatively to compare relative dissolution trends rather than absolute values.

Electrochemical measurements in full single-cell PEM water electrolyzer testing

Two titanium flow fields with serpentine channels (T3, v2.0, Dioxide Materials), each having an active area of 5 cm^2, were used as the anode and cathode plates. PTFE gaskets (Fuel Cell Store) with thicknesses of 0.13 ± 0.003 mm for the cathode and 0.27 ± 0.003 mm for the anode were employed. Asymmetric PTFE gaskets were selected based on the differing thickness and mechanical properties of the electrodes, with a platinized Ti-felt anode (~ 0.25 ± 0.003 mm) and a platinized carbon-cloth cathode (~ 0.40 ± 0.003 mm). The thinner cathode gasket ensures sufficient compression of the carbon cloth for good electrical contact, while the thicker anode gasket prevents over-compression of the porous Ti-felt, ensuring uniform sealing and stable cell assembly. A Nafion N115 membrane (4.5 × 4.5 cm^2, Ion power, UK), pre-soaked in deionized water for 24 h, was used as the proton-exchange membrane. The anode consisted of a Ru thin film deposited on platinized Ti-fiber felt (4.4 cm^2), serving as both the oxygen evolution reaction (OER) catalyst and gas-diffusion electrode (GDE). The air annealed sample (400 °C) was selected based on its three-electrode performance compared to the Ar annealed sample. The active anode area was 2.2 × 2.2 cm^2, with a Ru loading of 0.162 mg cm^{-2}. The cathode comprised Pt supported on Vulcan carbon cloth (2.5 × 2.5 cm^2), functioning as the hydrogen evolution reaction (HER) catalyst and GDE, with a Pt loading of 0.5 mg cm^{-2} and a thickness of ~ 0.40 ± 0.003 mm. The Ru-coated Pt/Ti felt, and Pt/C GDE were placed onto their respective flow fields, and the cell was assembled in a zero-gap configuration. Intimate contact between the electrodes, gaskets, and membrane was ensured by applying a torque of 2.5 Nm during cell assembly. This torque value was used in accordance with our established laboratory protocol to ensure reproducible sealing integrity and appropriate electrode compression across repeated assemblies. After cell assembly, a 30 min leak test was performed by introducing deionized water through both the anode and cathode sides under ambient conditions. The absence of visible leakage was used as the acceptance criterion prior to electrochemical measurements. The cell was subsequently evaluated at 60 °C with a controlled electrolyte flow rate of 30 mL min^{-1}. Polarization curves were obtained via linear sweep voltammetry (LSV), using a Biologic SP-150 potentiostat for low-current measurements and a Lahne potentiostat for high-current measurements.

3. Results and Discussion

Figure S1 summarizes all Ru sputtered Pt/Ti-felt electrodes investigated in this work, including annealing conditions, detected phases, and catalyst loading derived from the sputtered Ru thickness. It also outlines the electrode geometries used for three-electrode measurements and full PEM electrolyzer testing, along with the corresponding structural, compositional, and electrochemical characterizations performed for each sample. This provides a consolidated overview of the complete experimental

View Article Online
DOI: 10.1039/D6MA00277C

workflow and sample set. **Table S1** lists characterization performed and electrolyte used, providing a clear comparison of all electrode configurations. The surface morphology of the Pt/Ti-felt substrate and the sputtered Ru coatings was examined by SEM at different magnifications (**Fig. 1a–e**). The images reveal the characteristic porous, fibrous structure of the Ti felt, which is preserved after sputter deposition and subsequent annealing treatments. At the micron scale, the Ru coating appears to conformally cover the exposed fiber surfaces without significantly altering the overall morphology of the substrate. The SEM observations suggest consistent coating coverage across the fibers for both the as prepared and annealed samples (400 °C in air or argon). In addition, the Energy Dispersive X-ray Spectroscopy (EDS) maps confirm consistent Ru-distribution on the surface without any patches suggesting a homogeneous film (**Fig. 1b-f**), further confirmed by higher-resolution SEM (**Fig. S3**). A Pt signal was also detected due to the use of platinized Ti-felt, which was employed to ensure stable electrical contact and uniform current distribution; the thin Pt interlayer (~ 0.3 ± 0.1 at% by EDS) (**Fig. S2**) acts only as a conductive layer with negligible contribution to the overall composition. The atomic percentages of all relevant elements (Ti, Ru, Pt, and O) were mapped, and the values are reported as averages obtained from multiple mapped regions to provide a statistical representation of the surface composition. The measured compositions are: pristine Pt/Ti felt (Ti-99.7 ± 0.2 at%, Pt-0.3 ± 0.1 at%; as prepared (Ti- 53.30 ± 0.21 at%, Ru- 31.43 ± 0.35 at%, O- 11.77 ± 3.43 at%); 400 °C air annealed (Ti- 42.73 ± 1.22 at%, Ru- 36.53 ± 3.66 at%, O- 20.73 ± 2.66 at%); and 400 °C Ar annealed (Ti- 43.27 ± 1.48 at%, Ru- 33.40 ± 2.02 at%, O- 23.33 ± 2.37 at%). Based on AFM measurements on a co-deposited 300 nm – SiO_2/Si reference substrate, the Ru film thickness was estimated to be ~ 130 nm (**Fig. S4**), corresponding to a mass loading of 0.162 mg_{Ru} cm^{-2}. Hence, the total noble metal loading on the catalyst-coated substrate is dominated by Ru (0.162 mg cm^{-2}), while the Pt interlayer functions solely as a conductive adhesion and current-collection layer and is not intended to contribute to the oxygen evolution reaction under the investigated conditions.

Noteworthy, XRD patterns of the respective samples (**Fig. S5**), show that the diffraction peaks remain consistent with those of Ru metal, in good agreement with ICSD data 208029 [25]. The annealing has a minimal effect as evident from the striking similarity of diffraction patterns of all three samples (**Fig. S5**). This suggests that any structural change in the sample probably occurs only at the surface level. Hence, X-ray Photoelectron Spectroscopy (XPS) was carried out with the survey spectra (**Fig. S6**) showing a noticeable overlap between the Ru 3d and C 1s regions, which is a common issue.[26-28] Therefore, the high-resolution spectra were recorded in the Ru 3p region.

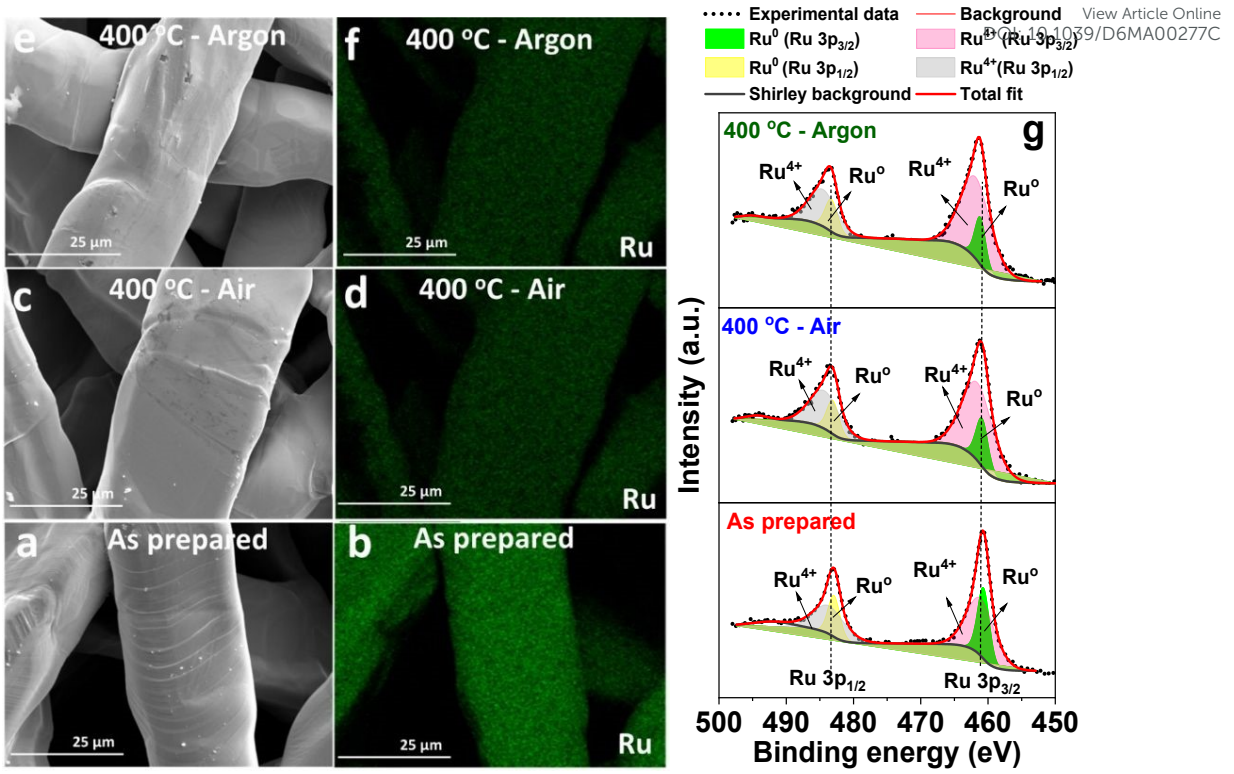

Figure 1: SEM micrographs of Ru sputtered thin films: Left panel **(a)** as prepared, **(c)** annealed at 400 °C in air, and **(e)** annealed at 400 °C in Ar. Right panel **(b, d, f)** present the associated EDS elemental maps for Ru. **(g)** High-resolution XPS spectra of the as prepared and annealed Ru film showing the Ru 3p features subjected to each annealing condition.

High-resolution XPS spectra of the Ru 3p region were collected for the as prepared and annealed films **(Fig. 1g)**, revealing contributions from both metallic Ru (Ru^0) and oxidized Ru species. For the as prepared film, the Ru $3p_{3/2}$ peaks are located at 460.68 eV (20.23 %) and 461.03 eV (40.08 %), while the Ru $3p_{1/2}$ peaks appear at 482.91 eV (12.18 %) and 483.63 eV (22.43 %) **(Table S2)**. After annealing at 400 °C in air, the Ru $3p_{3/2}$ peaks shift to 460.89 eV (12.47 %) and 461.53 eV (52.02 %), corresponding to positive shifts of +0.21 eV and +0.50 eV, respectively, relative to the as prepared film. A similar trend is observed for the Ru $3p_{1/2}$ region, with peaks at 483.07 eV (8.85 %) and 484.32 eV (24.43 %), indicating an increased contribution from higher binding energy components consistent with enhanced oxidation. Annealing in argon at 400 °C further shifts the Ru $3p_{3/2}$ peaks to 461.15 eV (11.29 %) and 461.81 eV (55.10 %), representing shifts of +0.47 eV and +0.78 eV, respectively, compared to the as prepared film, and +0.26 eV and +0.28 eV relative to the air annealed sample. The Ru $3p_{1/2}$ peaks similarly shift to 483.29 eV (9.06 %) and 484.54 eV (23.41 %). Subtle shifts in binding energy likely reflect differences in local chemical environment and coordination at the Ru surface. High-resolution Ru 3p XPS spectra can be deconvoluted into metallic (Ru^0) and oxidized (Ru^{4+}/low-valence Ru) components, with variations in binding energy typically attributed to changes in oxidation state and local electronic environment. For instance, XPS investigations of thermally oxidized Ru films reveal systematic shifts in Ru 3p core-level peaks as Ru is converted to RuO_2 with increasing temperature.[29]

View Article Online
DOI: 10.1039/D6MA00277C

Similarly, RuO_2 catalyst annealed under different thermal conditions exhibit progressive Ru 3p3/2 binding energy shifts, reflecting increasingly oxidized surface environments.[30] These mixed surface states can significantly influence the electronic structure and catalytic performance of the films.[31, 32]

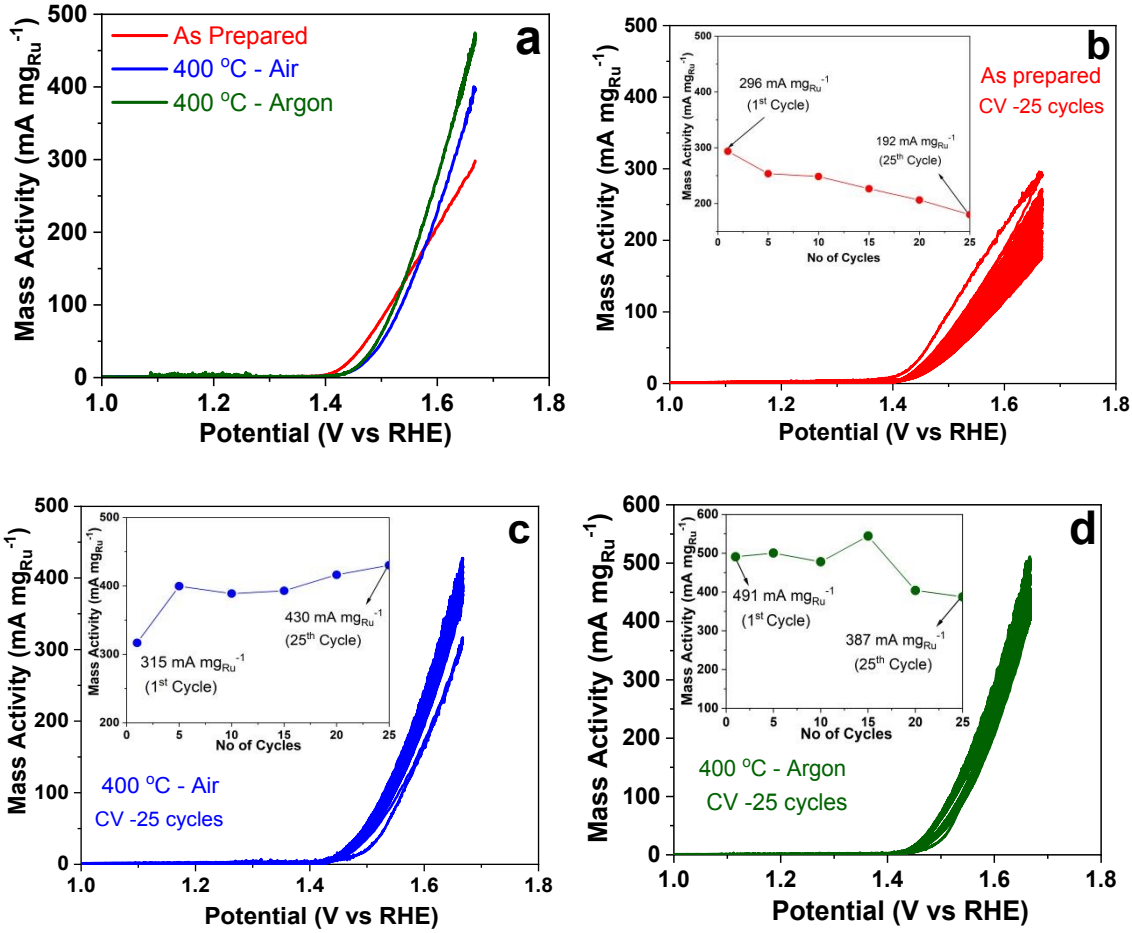

Figure 2: (a) LSV polarization and cyclic stability of the **(b)** as sputtered, **(c)** 400 °C-air annealed and **(d)** 400 °C-Argon annealed sputtered Ru thin films for 25 continuous cycles. Inset of **(b–d)** shows the mass activity values recorded at specific cycle numbers (5, 10, 15, 20, and 25). LSV polarization and CV curves are expressed in mass activity (mA mg_{Ru}^{-1}), normalized to the nominal Ru loading of 0.162 mg_{Ru} cm^{-2}.

Figure 2a presents the Linear Sweep Voltammetry (LSV) polarization curves for the as prepared and films annealed in air and argon at 400 °C. The annealing temperature of 400 °C was selected for both air and argon treatments based on preliminary screening and literature reports identifying 400 °C as an effective thermal treatment range reported for Ru-based OER catalysts.[33, 34] The currents were normalized by the Ru mass on each electrode (0.162 mg_{Ru} cm^{-2}, see **Supporting Information section 2 for details**) to estimate mass activity (mA mg_{Ru}^{-1}), allowing direct comparison between the films. Normalizing by Ru mass allows these intrinsic activity differences to be clearly distinguished, independent of variations in film thickness or loading, highlighting the impact of post-deposition treatment on catalytic behaviour. Despite identical catalyst loadings, the films show differences in performance. The as prepared Ru film exhibits the lowest overpotential for current onset but the lowest

View Article Online
DOI: 10.1039/D6MA00277C

mass activity at higher potentials. In contrast, the annealed films achieve enhanced mass activity of 60 mA mg_{Ru}^{-1} and 65 mA mg_{Ru}^{-1} at ~1.5 V vs. RHE for the air and Ar annealed films, respectively. These values are comparable to previously reported RuO_2 nanoparticles supported on Au and glassy carbon, which exhibited mass activities of ~ 100 - 600 mA mg_{Ru}^{-1} at ~1.5 V. [35] Ultrathin RuO_2 nanoskin films prepared by electroless deposition have also been reported to deliver mass-normalized OER activities of ~ 40 - 60 mA mg_{Ru}^{-1} at moderate overpotentials (~ 330 mV). [35] In this study, the sputtered Ru films have showed mass activities of 400 mA mg_{Ru}^{-1} and 475 mA mg_{Ru}^{-1} at ~ 1.65 V vs. RHE for the air and Ar annealed films, respectively. These results show that ultra-thin sputtered Ru films provide uniform, well-controlled coatings and high intrinsic mass activity in the three-electrode system, making them a potential benchmark for evaluating thin-film-based OER electrodes.

Evaluating the electrochemical efficacy of the sputtered Ru films as OER catalysts in a 3-electrode setup is crucial prior to their integration into a PEM flow-electrolyzer. RuO_2 and metallic Ru thin films are widely studied model systems because they offer among the highest intrinsic activities in acidic OER, but they exhibit a pronounced activity-stability trade-off. [36] For instance: Roy et al.,[10] investigated well-defined RuO_2 surfaces and particles under acidic OER conditions, finding that RuO_2 exhibits high activity but is also prone to dissolution, with activity and stability being surface-structure dependent across different crystal facets. In the current work, cyclic stability was evaluated by performing CV over 25 cycles between 1.0 and 1.65 V (vs RHE) at a scan rate of 5 mV s^{-1}.

The as prepared Ru film exhibits a significant decrease in mass activity over cycling (**Fig. 2b**). In contrast, films annealed in air (**Fig. 2c**) and argon (**Fig. 2d**) display improved stability, with mass activity increasing during repeated cycles. Especially, the air annealed films gradually develop active RuO_x sites through repeated CV cycles, ultimately achieving mass activity and durability comparable to Ar-annealed films. These observations are consistent with previous reports that Ru/RuO_2 thin films undergo surface oxidation and reconstruction under OER conditions, enhancing active site availability.[37] Similar trends have been reported, with metallic Ru electrodes exhibiting significant current decay during repeated CV cycling, while thermally oxidized Ru or RuO_2 films show smaller changes in current over repeated cycles.[38]

Time-dependent chronoamperometry (CA) was subsequently performed at a constant potential of 1.60 V vs RHE to determine the sputtered film's stability. The currents were again normalized to the Ru loading (0.162 mg cm_{Ru}^{-2}) to have direct correlation from the LSV polarization. **Figure 3a** shows that the as prepared film is highly unstable under oxidative conditions. This trend reflects the well-known activity-stability trade-off in RuO_2 systems, where high initial activity often correlates with increased dissolution. [10] However, both annealed films exhibit almost similar stability. Subsequent LSV was repeated after CA testing to examine changes in the electrochemical response of the catalyst films

View Article Online
DOI: 10.1039/D6MA00277C

(**Fig. 3b**). An increase in mass-normalized current was observed for the air annealed film (**Fig. 3c**), while a decrease was observed for the argon annealed film (**Fig. 3d**).

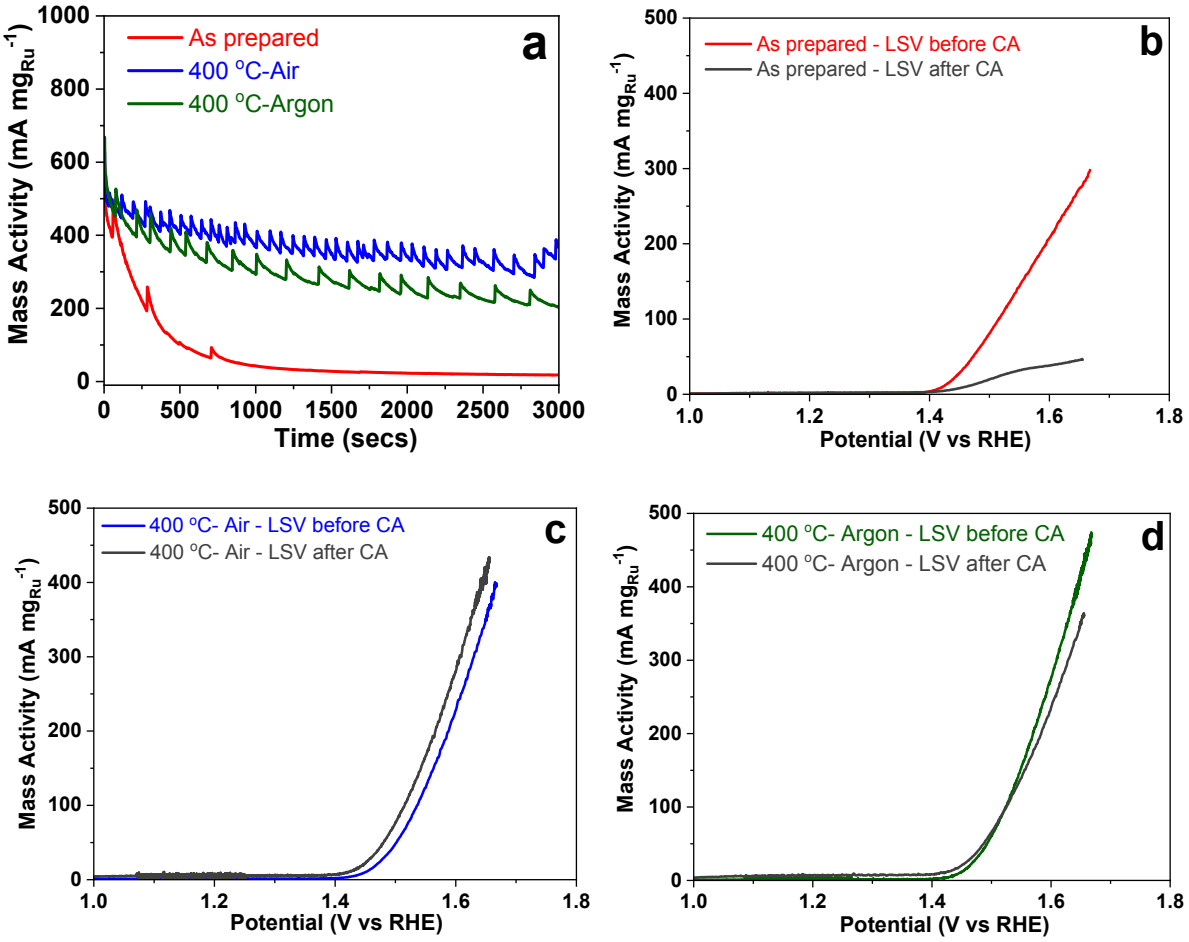

Figure 3: (a) CA stability curves of as prepared, air, and Ar annealed Ru films. LSV polarization curves of the **(b)** as sputtered, **(c)** 400 °C-air annealed and **(d)** 400 °C-Argon annealed sputtered Ru thin films before and after CA. CA and LSV polarization curves were expressed in mass activity (mA mg_{Ru}^{-1}), normalized to Ru loading of 0.162 mg_{Ru} cm^{-2}.

ICP analysis (**Table S3**) was performed after CA testing to quantify cumulative Ru dissolution. The 400 °C air annealed film shows slightly higher Ru dissolution than the argon annealed film, while the as-prepared film exhibits an intermediate value. Such behaviour is consistent with reports on Ru-based electrocatalysts showing that electrochemical stability and metal dissolution do not necessarily correlate directly, as Ru catalysts may undergo initial surface reconstruction and limited dissolution followed by formation of more stable surface structures. [39, 40] Accordingly, the 400 °C air annealed film exhibits the highest electrochemical stability in CA despite marginally higher cumulative Ru dissolution, indicating that air annealing promotes formation of a passivated oxide surface that suppresses further corrosion during prolonged operation. Overall, the electrochemical trends of the Ru-sputtered thin films correlate with XPS results, where increased RuO_x content after air annealing might have enhanced stability and reduced dissolution.

View Article Online
DOI: 10.1039/D5MA00277C

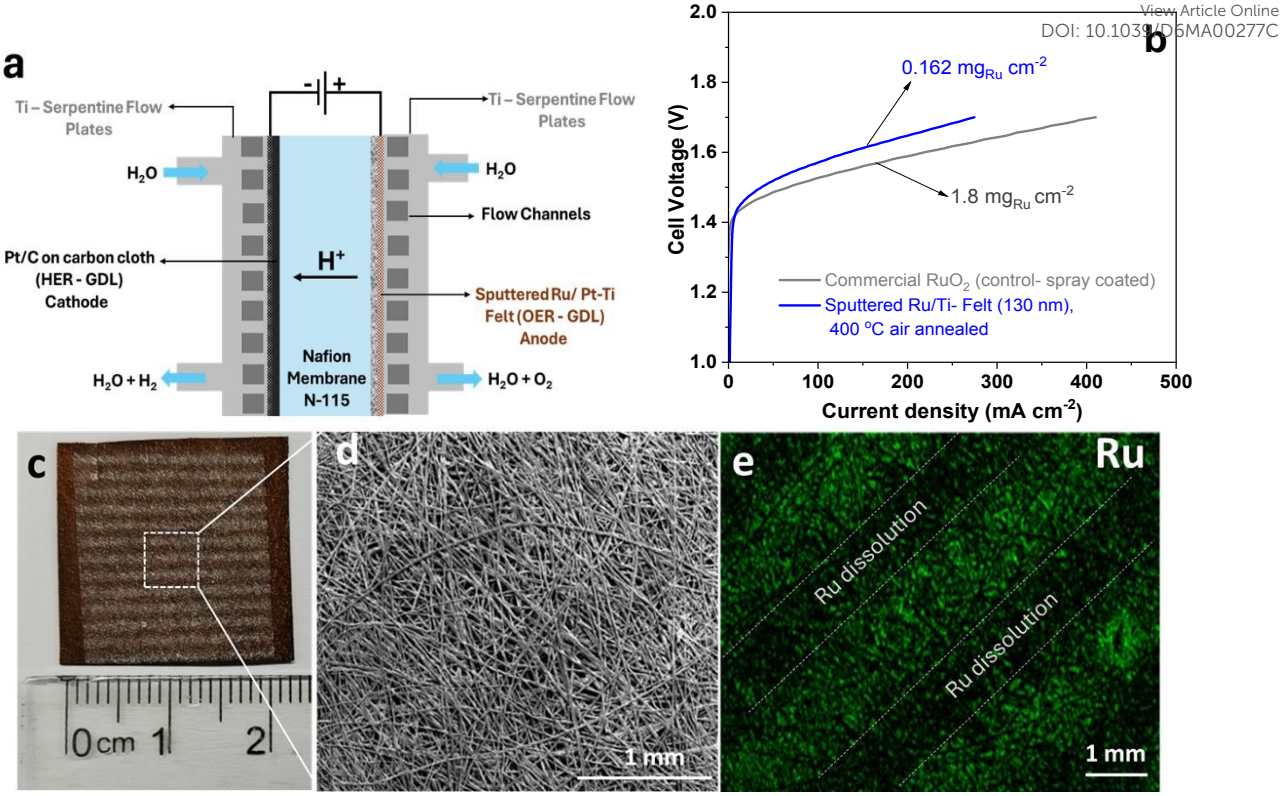

Figure 4: PEM electrolyzer testing was performed using a 400 °C air annealed Ru sputtered film as the anode. **(a)** Schematic illustration of the PEM cell configuration employing the 400 °C air annealed Ru sputtered film as the anode, Nafion-115 as a proton exchange membrane, and commercial Pt/C on carbon cloth as the cathode. **(b)** Polarization (I–V) curves comparing the performance of the low-catalyst-loaded (0.162 mg_{Ru} cm^{-2}) Ru sputtered film (blue line) with that of the commercial RuO_2 at a catalyst loading of 1.8 mg_{Ru} cm^{-2} (control anode). **(c)** Photograph of the Ru sputtered anode after post-electrolysis operation. **(d)** SEM image of the anode surface showing spatial dissolution of Ru along the serpentine flow-field channels, as confirmed by EDS analysis **(e)**.

To examine the relationship between 3-electrode measurements and device-level performance, a PEM electrolyzer was assembled (**Fig. S7**) using large-area sputtered Ru films deposited on the Pt/Ti felt and annealed in air at 400 °C was selected based on their electrochemical response in the 3-electrode configuration. A commercial gas diffusion electrode consisting of Pt/C supported on carbon cloth, procured from Fuel Cell Store, was employed as the cathode for the hydrogen evolution reaction (HER). Nafion-115 proton exchange membrane, obtained from Ion Power, was used as the proton-conducting separator (**Fig. 4a**). The electrolyzer was operated at 60 °C with a deionized water flow rate of 30 mL min^{-1}. After assembly, deionized water was circulated through the cell until the operating temperature reached 60 °C, which required approximately 30 min for stabilization.

Once stabilized, a polarization curve was recorded by scanning the cell voltage from 0 to 1.4 V at a scan rate of 5 mV s^{-1} (**Fig. S8a**). During this scan, a broad anodic feature was observed in the voltage range of approximately 0.5 – 0.9 V, consistent with electrochemical oxidation of Ru species. Anderson et al.,[37] observed broad redox peaks between ~ 0.6 and ~ 0.8 V, which are commonly attributed to the Ru^{3+}/Ru^{4+} redox couple for ruthenium oxides. Following the initial polarization measurement, the cell

View Article Online
DOI: 10.1039/D6MA00277C

voltage was increased to 1.5 V and the corresponding current response was recorded (**Fig. S8b**), resulting in an increase in current density. The cell was subsequently operated at a constant geometric current density of 50 mA cm^{-2} for 30 min (**Fig. S8c**). During this constant-current operation, the cell voltage increased by approximately 100 mV, rising from ~1.45 V at the beginning of the hold to ~1.55 V after 30 min. Gradual increases in cell voltage under sustained current loads have been reported in PEM water electrolyzers, where operating voltage drift is attributed to evolving internal resistances and electrode interface changes during galvanostatic operation.[41]

Subsequently, stepwise polarization experiments were performed with incrementally increased upper potential cutoffs of 1.60, 1.65, 1.70, and 1.75 V at a scan rate of 5 mV s^{-1} to suppress accelerated Ru dissolution associated with the initial exposure to elevated anodic potentials (**Fig. S8d**). The maximum current density close to 300 mA cm^{-2} was obtained for the Ru catalyst loading of 0.062 mg cm_{Ru}^{-2} during the scan with an upper voltage limit of 1.7 V (**Fig. 4b**).

To investigate the effect of Ru catalyst loading, a control anode electrode was prepared by spray-coating commercial RuO_2 onto the Ti felt (**Fig. 4b, grey curve**), resulting in a catalyst loading of ~ 1.8 mg_{Ru} cm^{-2} (**Supporting Information Section 3 for details**). The phase composition and morphology of the spray-coated RuO_2 electrode was characterized by XRD, SEM, and EDS mapping (**Fig. S9**). The electrochemical performance of this control electrode was compared with that of a Ru-sputtered Ti-felt electrode with a markedly lower Ru loading of 0.162 mg_{Ru} cm^{-2}, which was annealed at 400 °C in air (**Fig. 4b, blue curve**). At a current density of ~ 400 mA cm^{-2}, the control spray-coated RuO_2 electrode achieved a cell voltage of ~1.62 V, whereas the sputtered Ru film required ~1.70 V, corresponding to a voltage difference of ~ 80 mV. Despite this modest increase in overpotential, the Ru sputtered electrode delivers comparable current density with nearly 11-fold lower Ru loading, underscoring the effectiveness of sputter deposition in maximizing catalyst utilization. The sputtering process enables the formation of an ultrathin, conformal Ru coating with intimate electrical contact to the Ti felt, ensuring homogeneous current distribution and minimizing charge and mass transport resistances associated with thick, particulate catalyst layers. [42] Therefore, the objective of this study is not to replicate or compete with fully optimized commercial CCM-based PEM electrolyzers, but to evaluate the behaviour of ultra-thin low-Ru loading (0.162 mg cm^{-2}) in a CCS configuration under controlled operating conditions. This approach enables investigation of structure–property–performance relationships at reduced noble-metal loading compared to commercial RuO_2-based electrodes. Lower performance relative to CCM-based systems is expected due to differences in catalyst layer architecture, ionomer distribution, and interfacial design.

Similar trends have been reported for ultra-low Ru loading which achieve high electrocatalytic activity due to efficient utilization of active sites. [43] Direct reports of PEM water electrolyzer performance using metallic Ru thin-film anodes remain limited, but available data indicate moderate current densities at

View Article Online
DOI: 10.1039/D6MA00277C

low catalyst loading (**Table S4**). For instance: Hrbek et al.,[44] reported a pure Ru thin-film anode MEA achieving ~ 250 mA cm^{-2} at 2.0 V. In comparison, the sputtered Ru thin films demonstrate ~ 300 mA cm^{-2} at 1.7 V with only 0.162 mg cm_{Ru}^{-2} of Ru, illustrating superior site utilization. Commercial RuO_2-based MEAs typically require higher loadings (~ 1.8– 2 mg cm_{Ru}^{-2}) to reach similar or slightly higher current densities (400 –500 mA cm^{-2} at 1.7 – 1.8 V) [45, 46] , while high-temperature calcined RuO_2 prepared by sol-gel method achieves ~ 880 mA cm^{-2} at 1.8 V. [47] When scans were extended to higher upper voltage limits, lower current densities were measured in the subsequent polarization curves. Similar changes in polarization behaviour after exposure to higher anodic potentials have been reported for Ru-based OER catalysts, where operation at elevated potentials is accompanied by changes in electrochemical response and accelerated degradation. [10, 36]

Post-electrolysis examination of the Ru thin film anode revealed serpentine flow-field imprints (**Fig. 4c**) on the electrode surface, accompanied by localized reductions in Ru signal as confirmed by SEM/EDS elemental mapping (**Fig. 4d & e**). Such spatial heterogeneous changes in Ru signal intensity and morphology are consistent with the known susceptibility of ruthenium and its oxides to dissolution and over-oxidation under acidic OER conditions, a recognized challenge for Ru-based anodes in PEM water electrolysis. [48] Similar heterogeneous phenomena have been reported in PEM studies, where microscopic investigations reveal non-uniform structural and compositional changes in catalyst and transport layers, linked to local variations in electrochemical conditions and flow distribution.[49, 50] These effects are further influenced by flow-field design, as serpentine channels can induce locally heterogeneous current density, water delivery, and gas removal.[51, 52] Despite these challenges, sputtering offers precise control over film thickness, and catalyst distribution compared to electrodeposition and chemically mediated synthesis routes, which often suffer from non-uniform coverage, film overgrowth, and rough surface features. [22] Overall, the sputtered Ru thin films on the porous Pt/Ti-felt developed in this work exhibit high mass activity in the three-electrode configuration, indicating efficient utilization of active sites at ultralow loadings. When implemented as an anode in a PEM water electrolyzer, it delivered significant current density at lower voltage, comparable to those achieved with commercial RuO_2 electrodes employing substantially higher catalyst loadings (**Table S4**). The post-electrolysis analysis reveals that degradation is spatially non-uniform, with preferential Ru loss occurring along flow-field contact regions (**Fig. 4e**). This behaviour highlights the sensitivity of ultra-thin Ru coatings to local variations in current density, mass transport, and anodic potential distribution within practical PEM electrolyzer operation. Such observations underline that, while Ru-based systems can achieve high intrinsic activity at low loading, their long-term stability is strongly influenced by electrode architecture and operating conditions, which remain key challenges for CCS-type configurations. These results demonstrate that electrode architecture and deposition precision achieved through sputtering, making them a reliable benchmark catalyst-coated substrate (CCS) for PEM water electrolyzer.

View Article Online
DOI: 10.1039/D6MA00277C

4. Conclusion

Ultra-thin Ru films (130 nm) can be sputtered onto porous Ti-felt, creating PFSA-binder-free, low-loading (0.162 mg cm^{-2}) catalyst coated substrates for acidic OER evaluation. Post-deposition annealing clearly influenced the surface chemistry and electrochemical behaviour, where air annealed films performed better in three-electrode system than the as prepared and Ar annealed films. These annealed films also showed high mass activity, demonstrating that even at an ultra-low Ru loading, the catalyst surface is efficiently utilized, a key factor for reducing noble metal usage while maintaining performance. However, when tested in a PEM electrolyzer as a CCS architecture, the anodes exhibited localized voltage-dependent Ru dissolution, showing that the intrinsic instability of metallic or partially oxidized Ru under acidic OER conditions remains a major challenge. In this regard, this work highlights the gap between lab-scale testing and real PEM electrolyzer performance, showing that the magnetron-sputtered Ru thin-film platform provides a simple, well-defined system to study degradation and guide strategies for stabilizing low-loading Ru anodes under practical operating conditions.

Authors Contributions: Arun Kumar Samuel: conceptualization, methodology, investigation, formal analysis, writing - original draft, visualization. Zeliha Ertekin: conceptualization, methodology, writing - review & editing, supervision. Finlay Walton: investigation, data curation, formal analysis, writing - review & editing. Weihao Li: investigation, data curation, formal analysis, writing- review & editing. Finn Tierney: investigation, data curation, formal analysis, writing- review & editing. Isha Maini: investigation, data curation, formal analysis, writing- review & editing. Christopher Kelly: investigation, data curation, formal analysis, writing - review & editing. Scott Watson: investigation, data curation, formal analysis, writing – review & editing. David Moran: investigation, data curation, formal analysis, writing - review & editing. Ioannis Zeimpekis: methodology, writing - review & editing. Mark D. Symes: supervision, validation, methodology, writing - review & editing. Alexey Y. Ganin: conceptualization, validation, supervision, writing - original draft, writing - review & editing; corresponding author.

Conflicts of interest: The authors declare that they have no known financial or personal conflicts of interest that could have influenced the work reported in this paper.

Data availability: The data underpinning this study have been deposited in the University of Glasgow's Enlighten database under accession code: https://dx.doi.org/10.5525/gla.researchdata.xxxxx.

Supplementary information (SI): The supporting information provides detailed characterization and evaluation of ultra-thin Ru sputtered on platinized Ti-felt as an anode for PEM electrolyzers. SEM, AFM, XRD, and XPS analyses confirm the uniformity and structural stability of the Ru films under different annealing conditions. PEM cell testing with a commercial N-115 membrane and Pt/C cathode. Control experiments with commercial RuO_2 highlight the advantages of the sputtered films. ICP

View Article Online
DOI: 10.1039/D6MA00277C

analyses assess Ru retention after testing. Figures S1-S9 and Tables S1-S4 provide complete experimental and characterization details.

Acknowledgement: A.Y.G. and A.K.S. acknowledge funding from UKRI (1249). A.Y.G. also acknowledges support from EPSRC (EP/W03333X/1) for this work. MDS acknowledges support from EPSRC (EP/W033135/1) and thanks the Royal Society for a University Research Fellowship (URF\R\211007).

References:

1. C. R. Wang, J. M. Stansberry, R. Mukundan, H.-M. J. Chang, D. Kulkarni, A. M. Park, A. B. Plymill, N. M. Firas, C. P. Liu and J. T. Lang, *Chemical Reviews*, 2025, **125**, 1257–1302.
2. R. Vinodh, T. Palanivel, S. S. Kalanur and B. G. Pollet, *Energy Advances*, 2024, **3**, 1144–1166.
3. C. V. Pham, D. Escalera-López, K. Mayrhofer, S. Cherevko and S. Thiele, *Advanced Energy Materials*, 2021, **11**, 2101998.
4. C. Qiu, C. Sellers, Z.-Y. Wu, D. A. Cullen, E. Stavitski, A. Tayal, T.-U. Wi, M. Kodali, B. Erb and A. Smeltz, *Nature Nanotechnology*, 2025, **20**, 1787–1795.
5. J. Chen, Y. Ma, C. Cheng, T. Huang, R. Luo, J. Xu, X. Wang, T. Jiang, H. Liu and S. Liu, *Journal of the American Chemical Society*, 2025, **147**, 8720–8731.
6. J. Kang, Y. Fang, J. Yang, L. Huang, Y. Chen, D. Li, J. Sun and R. Jiang, *ACS Applied Materials & Interfaces*, 2025, **17**, 20519–20559.
7. X. Cao, J. Huo, L. Li, J. Qu, Y. Zhao, W. Chen, C. Liu, H. Liu and G. Wang, *Advanced Energy Materials*, 2022, **12**, 2202119.
8. J. Chen, J. Ma, T. Huang, Q. Liu, X. Liu, R. Luo, J. Xu, X. Wang, T. Jiang and H. Liu, *Angewandte Chemie International Edition*, 2025, **64**, e202503330.
9. J. Chen, Y. Ma, T. Huang, T. Jiang, S. Park, J. Xu, X. Wang, Q. Peng, S. Liu and G. Wang, *Advanced Materials*, 2024, **36**, 2312369.
10. C. Roy, R. R. Rao, K. A. Stoerzinger, J. Hwang, J. Rossmeisl, I. Chorkendorff, Y. Shao-Horn and I. E. Stephens, *ACS Energy Letters*, 2018, **3**, 2045–2051.
11. J. Tang, D. Guan, H. Xu, L. Zhao, U. Arshad, Z. Fang, T. Zhu, M. Kim, C.-W. Pao and Z. Hu, *Nature Communications*, 2025, **16**, 801.
12. J. A. Clayton and R. I. Walton, *Johnson Matthey Technology Review*, 2022, **66**, 393–405.
13. H. Kim, K.-R. Yeo, H.-Y. Park, J. H. Jang and S.-K. Kim, *Korean Journal of Chemical Engineering*, 2025, **42**, 3365–3378.
14. J. Lim, J. M. Klein, S. G. Lee, E. J. Park, S. Y. Kang, S. Maurya, W. E. Mustain, S. Boettcher and Y. S. Kim, *ACS Energy Letters*, 2024, **9**, 3074–3083.
15. H. Park, S. Harris and P. A. Kohl, *ACS Electrochemistry*, 2025, **1**, 2495–2502.

16. M. Chatenet, B. G. Pollet, D. R. Dekel, F. Dionigi, J. Deseure, P. Millet, R. D. Braatz, M. Z. Bazant, M. Eikerling and I. Staffell, *Chemical Society Reviews*, 2022, **51**, 4583–4762.
17. S. A. Lee, S. E. Jun, S. H. Park, K. C. Kwon, J. H. Kang, M. S. Kwon and H. W. Jang, *EES Catalysis*, 2024, **2**, 49–70.
18. J. Cho, K.-S. Kim, S. Kim, Y. Shao, Y.-T. Kim and S. Park, *Small Structures*, 2024, **5**, 2300276.
19. L. Titheridge, S. K. Sharma, A. Soisson, C. Roth and A. T. Marshall, *Current Opinion in Electrochemistry*, 2025, **49**, 101607.
20. E. Slavcheva, I. Radev, S. Bliznakov, G. Topalov, P. Andreev and E. Budevski, *Electrochimica Acta*, 2007, **52**, 3889–3894.
21. M. A. Iqbal, S. Singh, A. Singh and S. Shahgaldi, *Materials Advances*, 2026.
22. T. Hrbek, P. Kúš, Y. Kosto, M. G. Rodriguez and I. Matolínová, *Journal of Power Sources*, 2023, **556**, 232375.
23. P. Kúš, A. Ostroverkh, K. Ševčíková, I. Khalakhan, R. Fiala, T. Skála, N. Tsud and V. Matolin, *International Journal of Hydrogen Energy*, 2016, **41**, 15124–15132.
24. J. Murawski, S. B. Scott, R. Rao, K. Rigg, C. Zalities, J. Stevens, J. Sharman, G. Hinds and I. E. Stephens, *Johnson Matthey Technology Review*, 2024, **68**, 121–146.
25. E. A. Riesel, T. Mackey, H. Nilforoshan, M. Xu, C. K. Badding, A. B. Altman, J. Leskovec and D. E. Freedman, *Journal of the American Chemical Society*, 2024, **146**, 30340–30348.
26. D. J. Morgan, *Surface and Interface Analysis*, 2015, **47**, 1072–1079.
27. M. P. Browne, C. Dominguez, C. Kaplan, M. E. Lyons, E. Fonda and P. E. Colavita, *ACS Applied Energy Materials*, 2023, **6**, 8607–8615.
28. M. Schaefer and R. Schlaf, *Journal of Applied Physics*, 2015, **118**.
29. J. T. Diulus, B. Tobler, J. Osterwalder and Z. Novotny, *Journal of Physics D: Applied Physics*, 2021, **54**, 244001.
30. Y. Yuan, C. Liu, S. Liu, R. Ding and X. Yin, *CrystEngComm*, 2025, **27**, 4835–4843.
31. M. Escudero-Escribano, A. F. Pedersen, E. A. Paoli, R. Frydendal, D. Friebel, P. Malacrida, J. Rossmeisl, I. E. Stephens and I. Chorkendorff, *The Journal of Physical Chemistry B*, 2018, **122**, 947–955.
32. Z. Ruiz-Bernal, M. Á. Lillo-Ródenas and M. C. Román-Martínez, *Reaction Chemistry & Engineering*, 2024, **9**, 461–474.
33. T. Audichon, B. Guenot, S. Baranton, M. Cretin, C. Lamy and C. Coutanceau, *Applied Catalysis B: Environmental*, 2017, **218**, 385–397.
34. P. Ren, R. Wang, Z. Teng, T. Wang, Y. Yang, Z. Jia, H. Gao, C. Pu, B. Li and S. Tan, *International Journal of Hydrogen Energy*, 2024, **72**, 1049–1057.
35. E. A. Paoli, F. Masini, R. Frydendal, D. Deiana, C. Schlaup, M. Malizia, T. W. Hansen, S. Horch, I. E. Stephens and I. Chorkendorff, *Chemical Science*, 2015, **6**, 190–196.

36. S. Cherevko, S. Geiger, O. Kasian, N. Kulyk, J.-P. Grote, A. Savan, B. R. Shrestha, S. Merzlikin, B. Breitbach and A. Ludwig, *Catalysis Today*, 2016, **262**, 170–180.
37. N. Deka, T. E. Jones, L. J. Falling, L.-E. Sandoval-Diaz, T. Lunkenbein, J.-J. Velasco-Velez, T.-S. Chan, C.-H. Chuang, A. Knop-Gericke and R. V. Mom, *ACS Catalysis*, 2023, **13**, 7488–7498.
38. J. Y. Kim, J. Choi, H. Y. Kim, E. Hwang, H.-J. Kim, S. H. Ahn and S.-K. Kim, *Applied Surface Science*, 2015, **359**, 227–235.
39. L. Hou, X. Gu, X. Cui, J. Tang, Z. Li, X. Liu and J. Cho, *EES Catalysis*, 2023, **1**, 619–644.
40. Y. Tang, Y. Lin, Y. Zhang, M. Deng and L. Chen, *Materials Today Energy*, 2024, **43**, 101603.
41. Z. Su, J. Liu, P. Li and C. Liang, *Materials*, 2024, **17**, 1331.
42. C. C. Weber, J. A. Wrubel, L. Gubler, G. Bender, S. De Angelis and F. N. Buchi, *ACS Applied Materials & Interfaces*, 2023, **15**, 34750–34763.
43. R. G. Milazzo, N. Marino, G. Tranchida, C. Bongiorno, L. Pulvirenti, L. Fusto, G. G. Condorelli, S. A. Lombardo and S. M. S. Privitera, *ACS Applied Energy Materials*, 2025, **8**, 5698–5707.
44. T. Hrbek, P. Kúš, T. Košutová, K. Veltruská, T. N. Dinhová, M. Dopita, V. Matolín and I. Matolinova, *International Journal of Hydrogen Energy*, 2022, **47**, 21033–21043.
45. W.-X. Zheng, X.-X. Cheng, P.-P. Chen, L.-L. Wang, Y. Duan, G.-J. Feng, X.-R. Wang, J.-J. Li, C. Zhang and Z.-Y. Yu, *Nature Communications*, 2025, **16**, 337.
46. C. Wang and L. Feng, *Energy Advances*, 2024, **3**, 14–29.
47. V. Natarajan, S. Basu and K. Scott, *International Journal of Hydrogen Energy*, 2013, **38**, 16623–16630.
48. S. Lee, C. Yang, J. Choi, J. H. Jang, H. Jin, Y.-E. Sung and H. S. Park, *Journal of Materials Chemistry A*, 2025, **13**, 18327–18337.
49. S. Finger, B. Fritsch, M. Wu, L. Lahn, D. Hoffmeister, J. Will, O. Kasian, E. Spiecker, S. Thiele and A. T. Freiberg, *Energy & Environmental Science*, 2025, **18**, 9877–9894.
50. K. H. Rho, Y. Na, T. Ha and D. K. Kim, *Membranes*, 2020, **10**, 441.
51. R. Mu, X. Cao, Y. Zhang, Y. He and Z. Wang, *Processes*, 2025, **13**, 1553.
52. R. Lin, Y. Lu, J. Xu, J. Huo and X. Cai, *Applied Energy*, 2022, **326**, 120011.

View Article Online
DOI: 10.1039/D5MA00277C

Ultra-Thin Ru-Sputtered on Ti-Felt Gas Diffusion Layer as Anode for Proton Exchange Membrane Electrolyzer

Arun Kumar Samuel[a], Zeliha Ertekin[a], Finlay Walton[b], Weihao Li[a], Finn Tierney[a], Isha Maini[b], Christopher Kelly[a], Scott Watson[b], David Moran[b], Ioannis Zeimpekis[c,d], Mark D. Symes[a], Alexey Y. Ganin [a]*

[a] *WestCHEM, School of Chemistry, University of Glasgow, University Avenue, Glasgow G12 8QQ, United Kingdom*

[b]*James Watt School of Engineering, University of Glasgow, University Avenue, Glasgow G12 8QQ, United Kingdom*

[c]*School of Electronics and Computer Science, University of Southampton, Southampton, United Kingdom*

[d]*Optoelectronics Research Centre, University of Southampton, Southampton, United Kingdom*

**Corresponding Author: alexey.ganina@glasgow.ac.uk*

Authors Contributions: Arun Kumar Samuel: conceptualization, methodology, investigation, formal analysis, writing - original draft, visualization. Zeliha Ertekin: conceptualization, methodology, writing - review & editing, supervision. Finlay Walton: investigation, data curation, formal analysis, writing - review & editing. Weihao Li: investigation, data curation, formal analysis, writing- review & editing. Finn Tierney: investigation, data curation, formal analysis, writing- review & editing. Isha Maini: investigation, data curation, formal analysis, writing- review & editing. Christopher Kelly: investigation, data curation, formal analysis, writing - review & editing. Scott Watson: investigation, data curation, formal analysis, writing – review & editing. David Moran: investigation, data curation, formal analysis, writing - review & editing. Ioannis Zeimpekis: methodology, writing - review & editing. Mark D. Symes: supervision, validation, methodology, writing - review & editing. Alexey Y. Ganin: conceptualization, validation, supervision, writing - original draft, writing - review & editing; corresponding author.

Conflicts of interest: The authors declare that they have no known financial or personal conflicts of interest that could have influenced the work reported in this paper.

Data availability: The data underpinning this study will be deposited in the University of Glasgow's Enlighten database under accession code: https://dx.doi.org/10.5525/gla.researchdata.xxxxx.

Supplementary information (SI): The supporting information provides detailed characterization and evaluation of ultra-thin Ru sputtered on platinized Ti-felt as an anode for PEM electrolyzers. SEM, AFM, XRD, and XPS analyses confirm the uniformity and structural stability of the Ru films under

View Article Online
DOI: 10.1039/D6MA00277C

different annealing conditions. Electrochemical measurements, including LSV, CV, and chronoamperometry, demonstrate high catalytic activity and durability. PEM cell testing with a commercial N-115 membrane and Pt/C cathode. Control experiments with commercial RuO_2 highlight the advantages of the sputtered films. ICP analyses assess Ru retention after testing. Figures S1-S9 and Tables S1-S4 provide complete experimental and characterization details.